The 2.0 Å Structure of Malarial Purine Phosphoribosyltransferase in Complex with a Transition-State Analogue Inhibitor[†,‡]

Wuxian Shi,[§] Caroline M. Li,[§] Peter C. Tyler,[||] Richard H. Furneaux,[||] Sean M. Cahill,[§] Mark E. Girvin,[§] Charles Grubmeyer,[⊥] Vern L. Schramm,*[,§] and Steven C. Almo*[,§]

Albert Einstein College of Medicine, Bronx, New York 10461, Carbohydrate Chemistry Team, Industrial Research Ltd., Lower Hutt, New Zealand, and Temple University School of Medicine, Philadelphia, Pennsylvania 19140

Received March 22, 1999; Revised Manuscript Received April 15, 1999

ABSTRACT: Malaria is a leading cause of worldwide mortality from infectious disease. *Plasmodium falciparum* proliferation in human erythrocytes requires purine salvage by hypoxanthine−guanine−xanthine phosphoribosyltransferase (HGXPRTase). The enzyme is a target for the development of novel antimalarials. Design and synthesis of transition-state analogue inhibitors permitted cocrystallization with the malarial enzyme and refinement of the complex to 2.0 Å resolution. Catalytic site contacts in the malarial enzyme are similar to those of human hypoxanthine−guanine phosphoribosyltransferase (HGPRTase) despite distinct substrate specificity. The crystal structure of malarial HGXPRTase with bound inhibitor, pyrophosphate, and two Mg^{2+} ions reveals features unique to the transition-state analogue complex. Substrate-assisted catalysis occurs by ribooxocarbenium stabilization from the O5′ lone pair and a pyrophosphate oxygen. A dissociative reaction coordinate path is implicated in which the primary reaction coordinate motion is the ribosyl C1′ in motion between relatively immobile purine base and $(Mg)_2$−pyrophosphate. Several short hydrogen bonds form in the complex of the enzyme and inhibitor. The proton NMR spectrum of the transition-state analogue complex of malarial HGXPRTase contains two downfield signals at 14.3 and 15.3 ppm. Despite the structural similarity to the human enzyme, the NMR spectra of the complexes reveal differences in hydrogen bonding between the transition-state analogue complexes of the human and malarial HG(X)PRTases. The X-ray crystal structures and NMR spectra reveal chemical and structural features that suggest a strategy for the design of malaria-specific transition-state inhibitors.

Plasmodium falciparum is a causative agent of malaria, a disease with a mortality in excess of 1 million persons per year in tropical regions (*1*−*3*). Protozoan parasites, including *P. falciparum*, are deficient in de novo synthesis of purines and require base salvage pathways to obtain nucleotides for DNA and RNA synthesis. The purine phosphoribosyltransferases catalyze transfer of the 5-phosphoribosyl group from 5-phospho-α-D-ribofuranosyl-1-pyrophosphate (PRPP)[1] to salvage hypoxanthine, guanine, or xanthine to form intracellular IMP, GMP, or XMP and are critical enzymes in the purine salvage pathway (*4*; Figure 1). The significance of hypoxanthine salvage is demonstrated by the failure of *Plasmodia* to proliferate in human erythrocytes exposed to xanthine oxidase, an enzyme that removes hypoxanthine from the medium (*5*). An inhibitor of *Tritrichomonas foetus* HGPRTase is known to prevent parasite growth in culture (*6*).

Malarial HGXPRTase has a low K_m for purine bases, and the equilibrium lies far in the direction of nucleotide formation (Figure 1). Human HGPRTase is 44% identical to the malarial enzyme in amino acid sequence but does not use xanthine as substrate. Genetic deficiency of human HGPRTase causes the Lesch−Nyhan syndrome, characterized by mental dysfunction and hyperuricemia (*7*). Targeting the purine salvage pathway therefore requires inhibitors which are specific for the parasitic enzyme.

A new class of transition-state analogue inhibitors for malarial HGXPRTase, the immucillin 5′-phosphates, has been developed recently. The inhibitors are >1000-fold more powerful than any inhibitors previously reported for HG(X)PRTase (*8*). *N*-Ribosyltransferases are known to stabilize ribooxocarbenium ion transition states (*9*−*11*). ImmucillinHP and immucillinGP were designed to mimic the features expected for ribooxocarbenium transition states in malarial

[†] This work is supported by research grants from the NIH and by developmental funds from Industrial Research Ltd. The NMR resource is supported by an equipment grant from the NSF and the Howard Hughes Medical Institute Research Resources Program for Medical Schools.

[‡] The coordinates for malarial HGXPRTase in complex with immucillinHP, two Mg^{2+}, and pyrophosphate have been deposited with the Protein Data Bank, ID code 1cjb.

* To whom correspondence should be addressed at the Department of Biochemistry, Albert Einstein College of Medicine, 1300 Morris Park Ave., Bronx, NY 10461. E-mail: vern@aecom.yu.edu or almo@aecom.yu.edu.

[§] Albert Einstein College of Medicine.

[||] Industrial Research Ltd.

[⊥] Temple University School of Medicine.

[1] Abbreviations: HGXPRTase, hypoxanthine−guanine−xanthine phosphoribosyltransferase; HGPRTase, hypoxanthine−guanine phosphoribosyltransferase; HPRTase, hypoxanthine phosphoribosyltransferase; PRPP, 5-phospho-α-D-ribofuranosyl-1-pyrophosphate; immucillinHP, (1*S*)-1-(9-deazahypoxanthin-9-yl)-1,4-dideoxy-1,4-imino-D-ribitol 5-phosphate; immucillinGP, (1*S*)-1-(9-deazaguanin-9-yl)-1,4-dideoxy-1,4-imino-D-ribitol 5-phosphate.

10.1021/bi990664p CCC: $18.00
Published on Web 07/13/1999

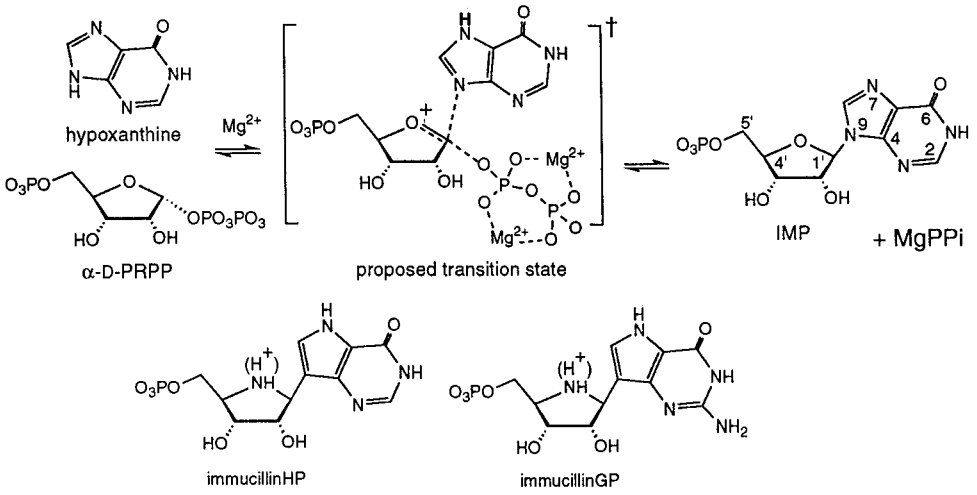

FIGURE 1: The phosphoribosyltransferase reaction of HGXPRTase with hypoxanthine is shown in the upper reaction. The K_{eq} for this reaction is 2×10^4 in favor of IMP formation (*22*). The proposed transition state with N7 protonation and a ribooxocarbenium ion is based on the transition states known for other *N*-ribosyltransferases (*9*−*11*). Transition-state analogues immucillinHP and immucillinGP are shown in the N4′-protonated forms. The pK_a values of 1-substituted iminoribitols are near 6.5 (*26*). The ionization status of N4′ when the inhibitors are bound to HG(X)PRTases is unknown. However, binding of related iminoribitols to nucleoside hydrolase occurs with unprotonated N4′ (*27*).

and human HG(X)PRTase. ImmucilinHP and immucillinGP are 1 and 14 nM transition-state analogues for malarial HGXPRTase while binding with dissociation constants of 2−5 nM to human HGPRTase (*8*; Figure 1). ImmucillinGP has been crystallized with the human HGPRTase with pyrophosphate and two Mg^{2+} bound at the active site. The structure of the complex provided the first view of a transition-state analogue inhibitor in the catalytic site of a phosphoribosyltransferase (*12*). The structure is unique in showing a complex with all loops closed and in close contact with the transition state inhibitor. Previous attempts to crystallize the malarial HGXPRTase have been thwarted by poor crystal growth. In the presence of immucillinHP, the enzyme crystallized readily. The crystals were formed at pH 7.5 with concentrations of Mg^{2+} and pyrophosphate that support full catalytic activity. The X-ray crystal structure of the malarial enzyme was solved to reveal the structural basis for inhibitor binding and to determine structural differences with the human enzyme. We report the 2.0 Å structure of the *P. falciparum* HGXPRTase in complex with immucillinHP. The structure identifies protein and Mg−pyrophosphate contacts that are important to the transition state and fulfills a long-held goal in antiparasitic drug design.

MATERIALS AND METHODS

Protein Purification and Crystallization. Recombinant HGXPRTase from *P. falciparum* was purified as described in ref *8*. A critical step in purification of the enzyme is removal of a persistent impurity with phosphatase activity. HGXPRTase was crystallized using hanging drop vapor diffusion at 18 °C. ImmucillinHP was dried onto the cover slip and 2 μL of 15−20 mg/mL HGXPRTase containing excess Mg^{2+}−pyrophosphate was mixed with 2 μL of mother liquid from the well containing 1 mL of 20% poly(ethylene glycol) 4000 (Fluka) and 100 mM, pH 7.5, Hepes (Sigma). These conditions achieved a 1:1.1 molar ratio of protein to inhibitor in the drop. The platelike crystals appeared in 3−5 days and grew to a maximum size of $0.5 \times 0.5 \times 0.1$ mm^3.

Data Collection and Processing. Data were collected from a single frozen crystal at −178 °C at the Brookhaven National Light Source, beamline X9B, and processed using DENZO (*13*). Diffraction from these crystals is consistent with the orthorhombic space group $C222_1$ ($a = 105.5$ Å, $b = 110.4$ Å, $c = 173.7$ Å). There are four subunit molecules in the asymmetric unit with $V_m = 2.2$ Å^3/Da and solvent content of 43%. The crystals diffracted to 1.65 Å but showed anisotropy beyond 2.0 Å. Data used for molecular replacement and structural refinement had a 99% overall completeness to 2.0 Å and R_{sym} of 4.8%. In the last shell (2.00−2.07 Å), 95% data has $I/\sigma I > 2.0$, with R_{sym} of 10.0%. Data collection and refinement statistics are summarized in Table 1.

Table 1: Data Collection and Refinement Statistics

resolution limits (Å)	20−2.0
no. of reflections	
unique	67609
total	286410
completeness (%)	99.1
R_{sym} (%, overall)	4.8
R_{sym} (%, 2.00−2.07 Å shell)	10.0
refinement statistics	
R_{cryst} (%)	19.6
R_{free} (%)	23.9
no. of amino acids	912
no. of waters	407
no. of ligands	4 ImmHP, 4 pyrophosphate, 8 Mg^{2+} ions
av protein *B*-factor (Å^2)	30.6
av ligand *B*-factor (Å^2)	24.2
av water *B*-factor (Å^2)	33.6
rms deviations, bond (Å)	0.006
rms deviations, angle (deg)	1.291

Molecular Replacement. The structure was solved by molecular replacement with the AmoRe software package implemented in CCP4 (*14*) using the crystal structure of human HGPRTase in complex with immucillinGP and Mg^{2+}−pyrophosphate as the search model (*12*). All amino acid side chains in the model that are different from the malarial HGXPRTase were trimmed to alanine, and the immucillinGP and Mg^{2+}−pyrophosphate were omitted from the search model. When the human dimer was used as a search model (human HGPRTase forms a tetramer in the crystal structure and the dimer with the largest buried surface

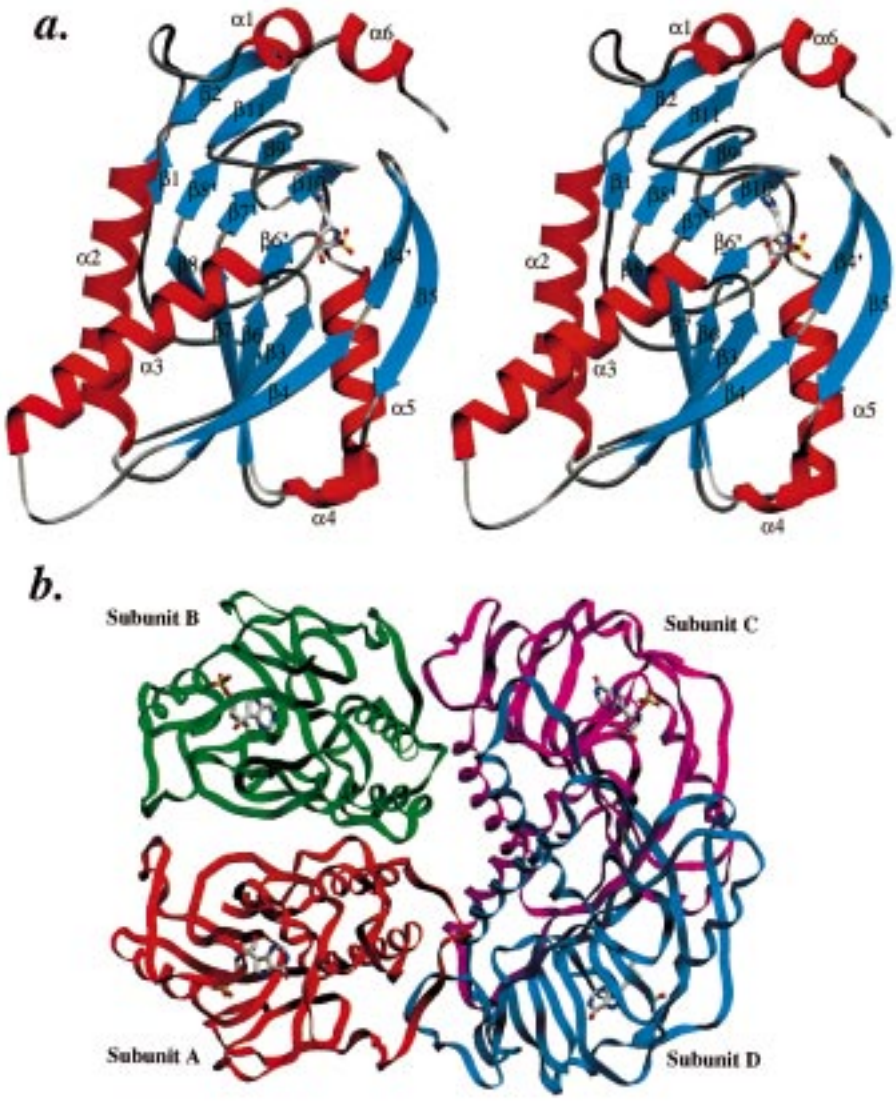

FIGURE 2: Views of the momomer and tetramer of malarial HGXPRT. (a) Stereoview of the monomer with bound immucillinHP. Helix α6 and sheets $\beta4'$ and $\beta5$ form the flexible hood and flap that cover the catalytic sites when inhibitor is bound. $\beta4'$, $\beta6'$, $\beta7'$, and $\beta8'$ are continuations of β-strands $\beta4$, $\beta6$, $\beta7$, and $\beta8$ but form separate β-sheets ($\beta6'$, $\beta7'$, $\beta8'$, and $\beta1$; $\beta4'$ and $\beta5$). The subunit packing (b) demonstrates the novel interfaces of the tetramer with the locations of the catalytic sites indicated with immucillinHP. Figures 2−5 were generated using Setor (*28*).

was used), three rotation and translation solutions were found with the correlation coefficients above the background. Subunit packing for the three solutions revealed that the dimers generated by two of the solutions are related by the crystallographic 2-fold axes. The final model included two molecules from solution 1 and one each from solutions 2 and 3. Malarial HGXPRTase forms a tetramer with 222 symmetry with one of the molecular 2-fold axes coincident with a crystallographic 2-fold axis. Consequently, the other two molecular axes are perpendicular to the crystallographic axis, and the four independent subunits in the asymmetric unit are contributed from two distinct homotetramers.

Structure Refinement. Rigid-body refinement (X-PLOR; *15*) of the model from AmoRe yielded an initial crystallographic *R*-factor and free *R*-factor of 48.5% and 47.0%, respectively, using 8.0−4.0 Å data. After one cycle of simulated annealing refinement, R_{cryst} and R_{free} dropped to 39.7% and 43.3%, and most of the missing side chains and the inhibitor had clear densities in $2|F_o - F_c|$ electron density maps. Strict noncrystallographic symmetry constraints were applied in the initial cycle of refinement, and the noncrystallographic symmetry restraints were relaxed gradually in the subsequent cycles. Bulk solvent and anisotropic *B*-factor corrections were subsequently applied. The loop segment of residues 95−105 (connecting α3 from $\beta4$; Figure 2) has three amino acid insertions relative to the human enzyme and was removed from the model in the early stage of refinement. The loop was built into omit maps in subsequent refinement cycles using the program O (*16*). Residues 2−13 are not present in the human HGPRTase structure (*12*) and were also built gradually into the electron density of the malarial enzyme. The final model includes residues 2−228 in subunits A, B, and D and residues 2−231 in subunit C, one immucillinHP, two Mg^{2+}, and one pyrophosphate for each subunit, and a total of 406 water molecules with R_{cryst} and R_{free} values of 19.6% and 23.9%, respectively. The model demonstrates excellent geometry determined by PROCHECK (*17*), with 90.6% in the most favored region, 7.9% in the additionally allowed region, 1.1% in the generously allowed region, and 0.5% in the disallowed region. Residue Asn66

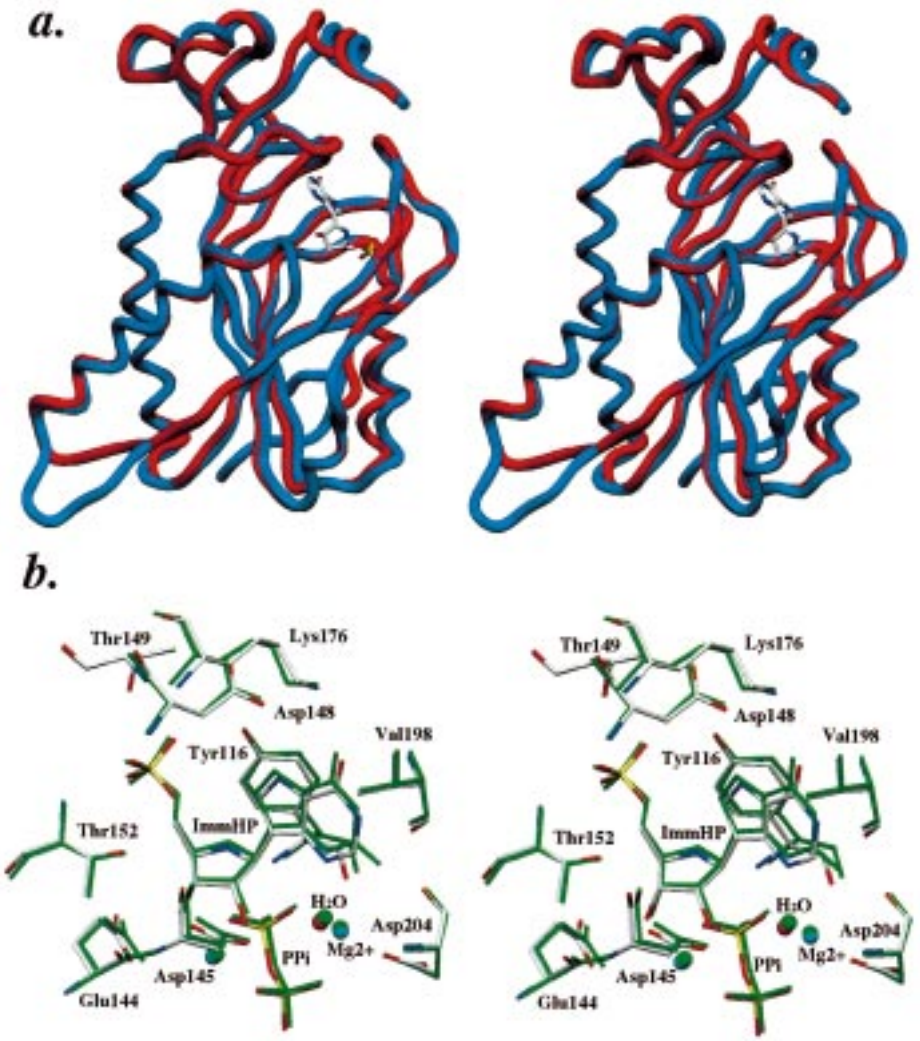

FIGURE 3: Stereoview comparison of human HGPRTase and malarial HGXPRTase with bound inhibitors. The rope diagram of the polypeptide backbones (a) shows one subunit of the malarial and human enzymes in blue and red, respectively. The extended loop and N- and C-terminal differences for the malarial enzyme reflect the 230 amino acids in the structure of the malarial enzyme compared to 217 amino acids in the human enzyme. The structure of immucillinHP is shown. In panel b, amino acid contacts to immucillinHP from the malarial enzyme are shown in gray, and those to immucillinGP from the human enzyme are shown in green. Both structures illustrate bound pyrophosphate and two Mg^{2+} ions (blue and green) and the ordered waters (red and green) located between Mg^{2+} and N3 of the bound inhibitors.

in the disallowed region is located in a loop and shows good density in the $|F_o - F_c|$ omit map.

RESULTS AND DISCUSSION

Overall Fold of Malarial HGXPRTase. The subunits of malarial HGXPRTase are folded into a single domain structure consisting of six α-helices and eleven β-strands (Figure 2a). A single subunit consists of a core (residues 46−194) and hood (residues 1−45 and 195−231) regions. The core is composed of a five-stranded parallel β-sheet (β4, 106−112; β3, 70−76; β6, 139−144; β7, 167−173; and β8, 187−190) surrounded by four α-helices (α2, 47−65; α3, 80−97; α4, 131−135; and α5, 151−163). Three strands from the central β-sheet are extended into a smaller four-stranded parallel β-sheet (β1, 17−19; β8′, 191−193; β7′, 174−176; and β6′, 145−147) located above the central β-sheet. The connection between β4 and α4 is made up of two antiparallel β-strands (β4′, 113−117; and β5, 120−127). These strands are folded directly over the bound transition-state inhibitor and serve to close the active site and sequester it from bulk solvent. The hood region is composed of two α-helices (α1, 34−39; and α6, 220−225) and a four-stranded antiparallel β-sheet (β2, 40−45; β11, 213−218; β9, 198−200; and β10, 203−205). The majority of the active site residues (144−152, 198−204) are located in β10 in the hood region and the loop connecting β6′ to α5 in the core region.

Quaternary Structure. The 222 symmetry of the tetramer generates three unique interfaces in the tetrameric structure (Figure 2b). The most extensive interface (A/B or C/D) buries a total of 2812 Å^2 surface area, which represents 12% of the total solvent-accessible surface area of a single subunit. Hydrogen bonds between main chain and side chain atoms of residues Lys38, Glu108, and Asp211 from subunit A are formed with Glu100, Lys77, Arg80, and Asn95 from subunit B. The other two interfaces (A/D, B/C and A/C, B/D) are less extensive and bury a total surface area of 1649 and 421 Å^2, respectively.

The four independent subunits in the asymmetric unit of the malarial HGXPRTase are remarkably similar with the root-mean-square deviation between all Cα atoms less than 0.5 Å in pairwise comparisons. Most of the differences occur in the loop regions, in particular, the loop connecting α3

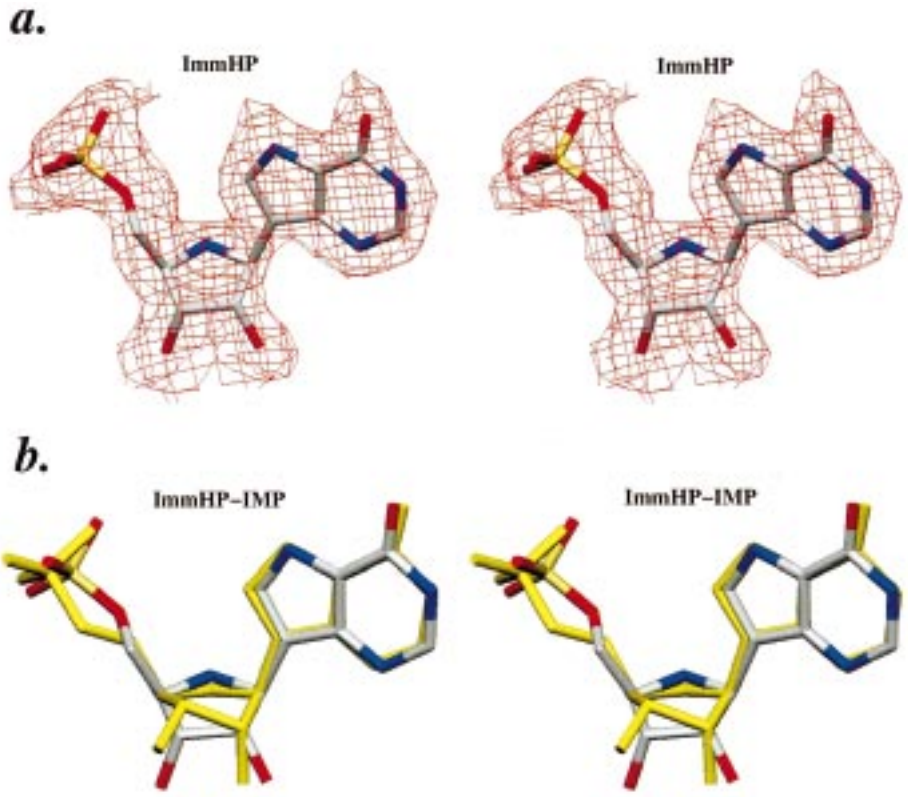

FIGURE 4: Stereoview of the electron density for immucillinHP at the catalytic site of malarial HGXPRTase (a). The $|F_o - F_c|$ omit electron density map was contoured at 2.0σ. The conformation of immucillinHP in the malarial enzyme (all bonds, gray; C, gray; N, blue; O, red; P, yellow) is compared to the conformation of IMP bound in the binary Michaelis complex with human HGPRTase (yellow) (b, *20*).

and β4 (98−105) and the loop connecting β5 and α4 (128−130). Excluding a total of 35 loop residues from the comparisons between Cα atoms reduces the root-mean-square deviation to less than 0.15 Å. The active sites in the four independent subunits are nearly identical with the root-mean-square deviation between Cα atoms of the active site residues (77−78, 115−116, 144−152, 176, 198−204) less than 0.10 Å. The tightly closed catalytic loop structures observed in all four subunits of the malarial HGXPRTase have been seen in only one previous purine phosphoribosyltransferase, that of human HGPRTase with a transition-state analogue inhibitor (*12*). The structure of the most closely related purine phosphoribosyltransferase from another organism is that of the HPRTase from *Trypanosoma cruzi* in complex with the purine analogue base from formycin B, PRPP, and two Mg^{2+} filling the catalytic sites (*18*). However, in this dimeric enzyme, the loop that closes over the catalytic sites (corresponding to β4′−β5 in Figure 2) is closed in only one of the two subunits. The loop closures are tighter in the malarial HGXPRTase than in the *T. cruzi* complex as evidenced by the distance from the general acids (Asp148 and Asp115, respectively) to N7 of the purine base. In the malarial enzyme, the distance is 2.8 Å in all subunits and generates a downfield H-bond at 14.3 ppm (see below). In the *T. cruzi* structure, these groups are separated by 4.1 and 3.3 Å in the two subunits (*18*). The overall similarity in all other portions of these structures indicates that the difference in the loop position is due to the presence of the transition-state inhibitor and not the difference in amino acid sequence of these enzymes.

Structure of the Catalytic Site. The 2.0 Å structure of malarial HGXPRTase reveals immucillinHP, pyrophosphate, and two Mg^{2+} bound at each of the four active sites of the tetramer (Figure 3b). The catalytic loops corresponding to residues 110−125 (β4′ and β5 in Figure 2a) are well ordered and are closed over every catalytic site. The $|F_o - F_c|$ omit maps show a well-defined electron density corresponding to full site occupancy with immucillinHP, pyrophosphate, and Mg^{2+}. Electron density for immucillinHP demonstrates the purine ring analogue in a low-antiglycosidic torsion angle (near 180°), similar to the angle for bound substrates (*20*, *21*; Figure 4).

Ribooxocarbenium ion transition states of *N*-ribosyltransferase reactions are characterized by unique structural and electronic features including (1) substantial positive charge at C1′−O4′ of the ribose ring, (2) a sp^2-hybridized C1′, and (3) a 3′-exo ribosyl ring pucker compared to a 3′-endo conformation in free nucleotides (*9*−*11*, *19*). The ribosyl ring pucker of immucillinHP in malarial HGXPRTase is 3′-exo, with 5′O cis to N4′ compared to that reported for IMP or GMP in crystals of human HGPRTase (*20*, *21*), which is 3′-endo, 5′O trans to O4′ (Figure 4b). Enzymatic contacts enforcing the ribooxocarbenium geometry include hydrogen-bonding interactions between the O2′ and O3′ hydrogens of the iminoribitol ring to Glu144 and Asp145 (2.7 and 2.5 Å). The outer Mg^{2+} ion is coordinated to both O2′ and O3′ oxygens at 2.2−2.3 Å and positioned below the plane of the iminoribitol ring. These interactions have the combined effect of restricting the positions of the 2′ and 3′ carbons of the sugar. The 5′-phosphate group of the transition-state

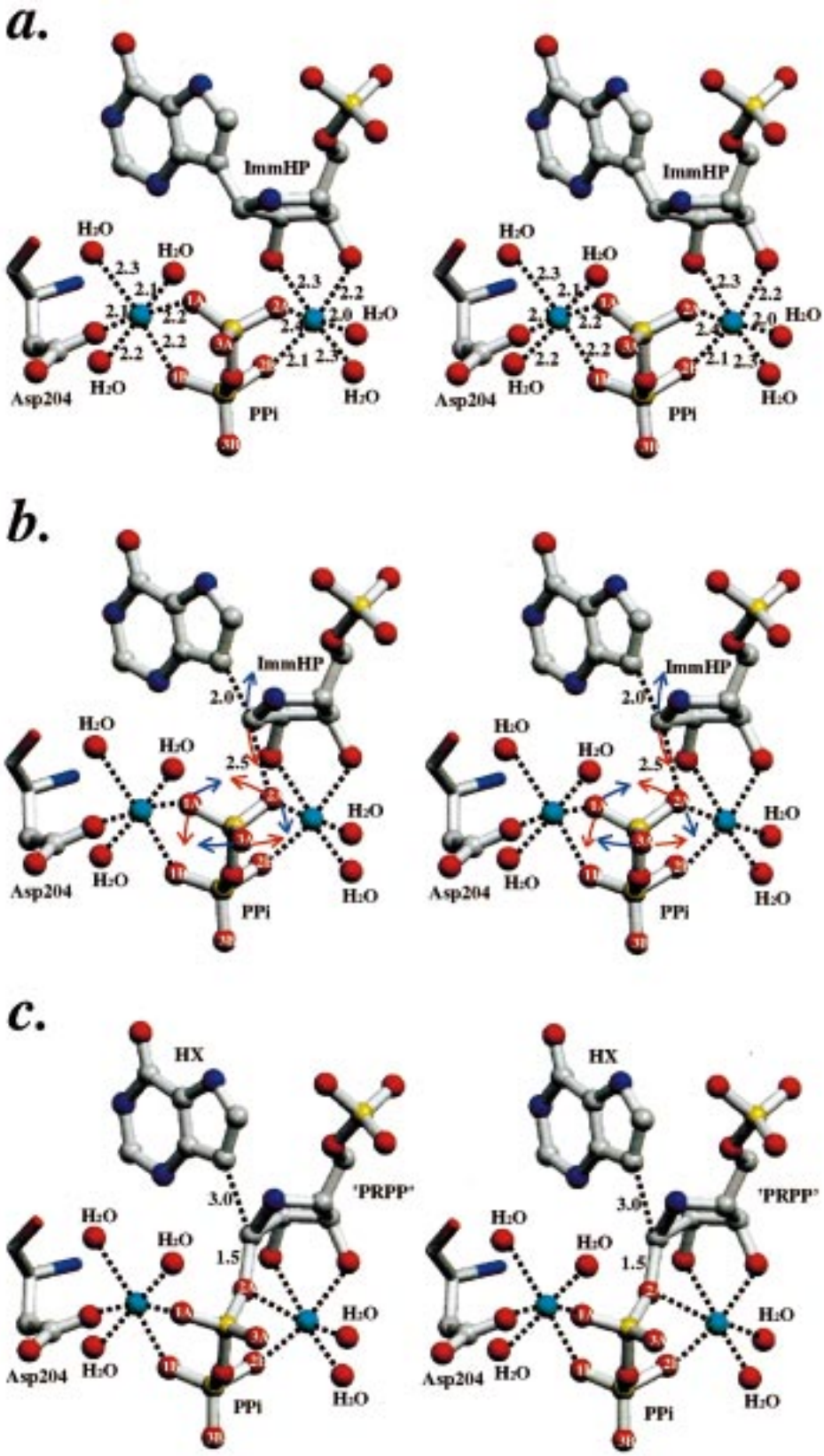

FIGURE 5: Stereoview of the contacts between malarial HGXPRTase and the Mg^{2+}−pyrophosphate complex. In (a), the distance is in angstroms between the Mg^{2+} (blue) and the oxygen of water, inhibitor, or enzyme (red). The reaction coordinate motion is proposed in (b). Separation of the C1′ carbon from the purine analogue to 2.0 Å generates a distance of 2.5 Å to O2A, the nearest oxygen of the pyrophosphate. Transition-state structures of nucleoside hydrolases give a similar N to C1′ distance near 3.0 Å to the phosphorus nucleophile (*8*−*10*). This observation suggests that the complex of immucillinHP and Mg^{2+}−pyrophosphate compresses the reaction coordinate distances nearer to that found in the transition state than in the fixed position of nitrogen−C1′−oxygen in Michaelis complexes. Rotation of the A phosphoryl group by approximately 10° counterclockwise (red arrows) brings O2A into an appropriate position for attack on the ribooxocarbenium ion. The motion proposed for the reaction between hypoxanthine and PRPP to form IMP and pyrophosphate is shown in blue arrows. In (c), PRPP geometry was generated by translocation of C1′ toward O2A and rotation of the A phosphoryl. The other atoms are the same as in (a).

analogue is immobilized by hydrogen bonds to the peptide amides of Asp148, Thr149, Gly150, and Thr152. Additional hydrogen bonds form with hydroxyl groups of Thr149, Thr162, and Tyr116. Tyr116 is brought to the catalytic site by the catalytic loop that closes in the presence of inhibitor. The final contacts to the 5′-phosphate group are provided by two ordered water molecules. Nine hydrogen bonds to the three 5′-phosphoryl oxygens (three to each oxygen) suggest a fixed, immobile group through the events of the reaction coordinate.

Immobilization of the 9-deazahypoxanthine ring results from Lys176 and Asp148 in hydrogen bonds to O6 and N7 of the ring. Val198 is in a carbonyl hydrogen bond to N1, and Asp204 stabilizes a $Mg^{2+}-H_2O$ 2.6 Å from N3, preventing purine ring motion toward the pyrophosphate. A network of hydrogen bonds between the protein, water, Mg^{2+}, and pyrophosphate restrict the pyrophosphate from motion toward the C1′ of iminoribitol. The two Mg^{2+} ions show nearly perfect octahedral coordination on opposite sides of pyrophosphate forming almost symmetric, bidentate interactions. The outer Mg^{2+} ion is located between the pyrophosphate and the iminoribitol ring of immucillinHP with distances to the six chelating atoms ranging from 2.4 to 2.1 Å (Figure 5). This Mg^{2+} ion does not directly contact any protein atom, but backbone atoms of Leu76, Val113, and the carboxyl of Glu144 participate in water-mediated interactions. The inner Mg^{2+} ion is coordinated to O2A and O2B of pyrophosphate, three water molecules, and Asp204, the only amino acid directly involved in Mg^{2+} binding. Mutation of this Asp in human HGPRTase (Asp193) causes Lesch−Nyhan syndrome, supporting its catalytic role. The network of protein−ligand interactions in the catalytic site is summarized in Table 2 and is compared to human HGPRTase.

Proposal for Reaction Coordinate Motion. The environment of immucillinHP and Mg^{2+}−pyrophosphate in the catalytic site of malarial HGXPRTase permits an interpretation of the translational freedom which allows reaction coordinate motion. Atomic movement is required to form the transition-state complex and is revealed in this structure. In the reaction coordinate, C1′ is free to translate from the purine base toward the pyrophosphate oxygen. As C1′ reaches the transition-state position near the midpoint of the translocation, the bonding electrons remain with the purine, and the purine charge is neutralized by a 2.8 Å hydrogen bond interaction between N7 and Asp148. This interaction has been assigned as a downfield hydrogen bond in the complex with [7-^{15}N]immucillinHP and Mg^{2+}-pyrophosphate (*8*). The ribosyl group becomes a ribooxocarbenium ion stabilized by the neighboring oxygens of the pyrophosphate from below and by the 2.7 Å distance to the lone pair electrons of O5′, directed toward O4′ by the 5′-phosphate interactions. A rotation of only 10° of the nearby phosphoryl group places the nucleophilic O2A oxygen directly under the highly reactive carbenium carbon. This rotation does not cause a significant change in the chelate bond lengths between O1A and O2A to the Mg^{2+} ions but brings C1′ and O2A within 2.5 Å, a distance consistent with the attacking oxygen nucleophiles in transition-state structures of *N*-nucleoside hydrolase and transferase reactions (*9*−*11*). The O2A pyrophosphate oxygen is most favorably positioned for a nucleophilic role and is in the weakest coordination with the catalytic site Mg^{2+} ions, at 2.4 Å, facilitating its translocation from the metal to the carbenium carbon (Figure 5).

Table 2: Comparison of Hydrogen Bond Distances in Malarial HGXPRTase−ImmucillinHP and Human HGPRTase−ImmucillinGP Complexes

	atom 2	residue	distance/ malarial	distance/ human
atom 1, ImmHP				
O1P	N	Gly150	3.0	2.8 (Gly139)
	N	Asp148	2.9	3.1 (Asp137)
	OH2	water	2.9	2.7
O2P	N	Thr152	2.8	2.7 (Thr141)
	OG1		3.0	2.8
	OH2	water	2.7	2.8
O3P	N	Thr149	3.0	2.9
	OG1		2.8	2.6 (Thr138)
	OH	Tyr116	2.6	2.8 (Tyr104)
O5′	N4′	ImmHP	2.7	2.7 (ImmGP)
O3′	OE2	Glu144	2.7	2.7 (Glu133)
O2′	OD1	Asp145	2.5	2.5 (Asp134)
N4′	O2A	PP_i	3.1	3.3
	O5′	ImmHP	2.7	2.7 (ImmGP)
N7	OD2	Asp148	2.8	2.8 (Asp137)
O6	NZ	Lys176	2.9	2.7 (Lys165)
N1	O	Val198	2.5	2.7 (Val187)
N3	OH2	water	2.6	2.7
N2 (ImmGP)	O			2.8 (Val187)
	O			2.8 (Asp193)
atom 1, PP_i				
O2A	N4′	ImmHP	3.1	3.3 (ImmGP)
O3A	N	Ser115	2.8	2.7 (Ser103)
	N	Tyr116	2.8	2.8 (Tyr104)
O2B	N	Gly78	2.8	2.8 (Gly69)
O3B	N	Lys77	2.9	3.1 (Lys68)
O3B	OH2	water	3.0	2.6
	OH2	water	3.0	2.8
O1B	NH2	Arg210	2.8	2.7 (Arg199)
	NH1		3.2	2.8
Mg^{2+} (I)	O2′	ImmHP	2.2	2.1 (ImmGP)
	O3′	ImmHP	2.3	2.3 (ImmGP)
	O2A	PP_i	2.4	2.5
	O2B	PP_i	2.1	2.1
	OH2	water	2.0	2.2
	OH2	water	2.3	2.2
Mg^{2+} (II)	O1A	PP_i	2.2	2.1
	O1B	PP_i	2.2	2.2
	OD1	Asp204	2.1	2.1 (Asp193)
	OH2	water	2.3	2.1
	OH2	water	2.1	2.2
	OH2	water	2.2	2.3

Pyrophosphate is located beneath the iminoribitol ring of immucillinHP 3.1−3.2 Å from C1′ but is restrained from translocating toward C1′ in a nucleophilic displacment. Backbone nitrogens from Ser115 and Tyr116 form favorable hydrogen bonds to O3A of pyrophosphate (2.7 and 2.8 Å). Oxygens 1A, 1B, 2A, and 2B are chelated directly to two Mg^{2+} ions, giving a large effective mass for the $(Mg)_2-$pyrophosphate$-H_2O$ complex. Pyrophosphate oxygens distal to the inhibitor are anchored by interactions with the side chain of Arg210 and the backbone nitrogen atom of Lys77. A rare cis peptide bond between Leu76 and Lys77 orients the backbone amide nitrogen atom toward pyrophosphate to form hydrogen bonds and the side chain ϵ-amino nitrogen to the A/B dimer interface to interact with the backbone oxygen of Glu108 in the neighboring subunit. Leu76 and Lys77 are conserved throughout the human and parasitic HGPRTases and are in cis peptide bonds in human HGPRTase with immucillinGP and in HPRTs from *T. cruzi* and

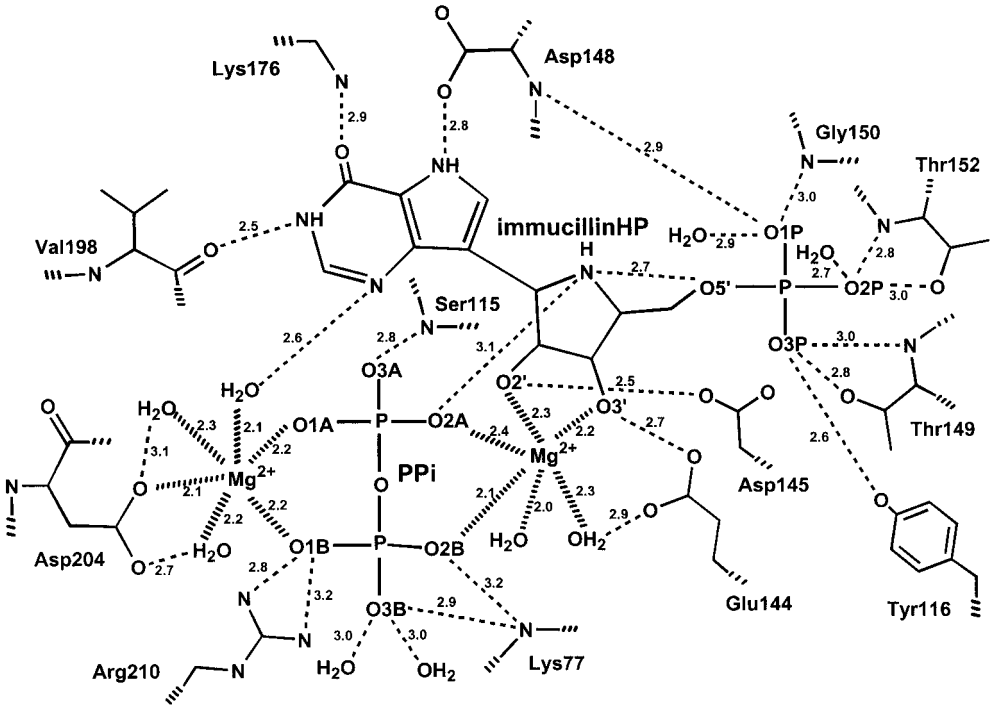

FIGURE 6: Distances for noncovalent interactions between the enzyme, Mg^{2+}−pyrophosphate, and the bound immucillinHP.

T. foetus (*6*, *12*, *18*). The net effect of these interactions is to restrict the translational motion of pyrophosphate toward C1′. In contrast to the tight anchoring of the 5′-PO_4 and 2′- and 3′-hydroxyls of the ribosyl, there are surprisingly few close contacts to C1′ and O4′. This geometry permits facile departure of C1′ toward O2A. A dissociative reaction mechanism is defined by this motion and results in formation of a ribooxocarbenium ion transition state. This proposal is illustrated in Figure 5b, where all atoms of the catalytic site are fixed except for a 0.5 Å motion of C1′ away from the purine analogue toward O2A of pyrophosphate. This motion generates a dissociative transition state closely related to those known to exist in other *N*-ribosyltransferases (*9*−*11*).

Comparison of Human and Malarial HG(X)PRTases. The malarial HGXPRTase structure is compared to the human HGPRTase in Figure 3 (*12*). All amino acid residues that are in contact with bound immucillins, pyrophosphate, and Mg^{2+} are conserved, and the active site complexes are closely related, even though the human structure was solved with bound immucillinGP and the malarial enzyme with immucillinHP. In the human HGPRTase complex, the carbonyl oxygens of Val187 and Asp193 (Val198 and Asp204 in the malarial enzyme) hydrogen bond with the C2-amino group of immucillinGP (not present in immucillinHP). Xanthine, in which a 2-oxo group replaces the amino group in guanine, is a substrate only for the malarial enzyme. It has been proposed that a water molecule might be involved in substrate recognition of the xanthine base to accommodate the change of a hydrogen bond donor in guanine to a hydrogen bond acceptor in xanthine. Several water molecules are located in this region but are conserved in both the malarial HGXPRTase complex with immucillinHP and the human HGPRTase complex with immucillinGP (Table 2). The hydrogen bonds between the malarial HGXPRTase and immucillinHP and $(Mg)_2$−pyrophosphate are summarized in Figure 6.

NMR Comparison of Downfield Proton Signals in HGXPRTase and HGPRTase. The near identity of the human and malarial HG(X)PRTase contacts to the immucillins was unexpected because of the difference in substrate specificity for xanthine. While the X-ray structure provides detail of catalytic site contacts, its accuracy is limited at the resolution needed for reliable prediction of short hydrogen bond interactions. Proton NMR spectroscopy has the required sensitivity to resolve these differences. The spectra collected at 600 MHz for human and malarial enzymes in complex with immucillinHP−Mg−pyrophosphate show significant differences (Figure 7).

ImmucillinHP alone and human HGPRTase or malarial HGXPRTase show no ^{1}H signals downfield of 12.7 ppm. Addition of immucillinHP alone or Mg^{2+}−pyrophosphate alone also reveals no downfield ^{1}H signals. The transition-state analogue ensemble results in new downfield ^{1}H signals for both malarial and human enzymes. The temperature dependence of the downfield peaks results in narrower line width as temperature increases, establishing that these protons are in slow exchange with solvent (*8*).

Two ^{1}H signals downfield of 13.5 ppm are detected in both enzyme−immucillinHP−Mg^{2+}−pyrophosphate complexes. In human HGPRTase, two complex-specific protons appear at chemical shift values of 13.9 and 15.6 ppm, while those of the malarial enzyme complex are at 14.3 and 15.3 ppm. The ^{1}H signals at 13.9 and 14.3 ppm have been assigned to the N7 proton of immucillinHP hydrogen bonded to Asp148 (Asp137 for the human enzyme) by ^{15}N-edited proton NMR spectra using [7-^{15}N]immucillinHP, while the most downfield protons are unassigned (*8*). This Asp contributes to k_{cat} but not significantly to substrate binding (*22*). A correlation has been established between chemical shift and hydrogen bond distance (*23*, *24*). Small changes in hydrogen bond distance are energetically significant (*25*). The downfield proton chemical shift differences observed

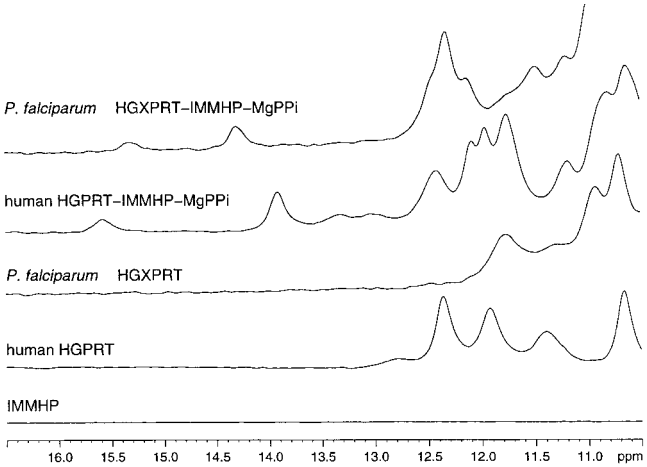

FIGURE 7: NMR spectra for immucillinHP (lower), human HGPRTase and *P. falciparum* HGXPRTase without added ligands (second and third from the bottom), and enzyme samples in complex with immucillinHP and Mg^{2+}−pyrophosphate. The enzyme was present at 0.7 mM and immucillinHP at 1 mM with excess Mg^{2+}−pyrophosphate. Spectra were collected at 600 MHz and 30 °C, using a 1-1 pulse sequence (*29*) and a total of 4096 transients. Proton chemical shifts were referenced to internal 3-(trimethylsilyl)propionate.

between the human and malarial HG(X)PRTase complexes establish different energetic contributions to the N7 hydrogen bonds for the human and malarial HG(X)PRTase complexes. The hydrogen-bonding properties of immucillins can be altered by the chemical substitution of electron-withdrawing or -donating groups. Substituted immucillins are expected to exhibit altered hydrogen-bonding potential, to interact differently with the enzymes. These inhibitors may have potential as isozyme-specific inhibitors against malaria.

ACKNOWLEDGMENT

We thank Dr. M. R. Chance (Albert Einstein College of Medicine, National Synchrotron Light Source supported by DOE) for the opportunity to collect X-ray data at beamline X9B, supported by RR01633.

REFERENCES

1. Nabarro, D. N., and Tayler, E. M. (1998) *Science 280*, 2067−2068.
2. Brundtland, G. H. (1998) *Science 280*, 2027a.
3. Mons, B., Klasen, E., van Kessel, R., and Nchinda, T. (1998) *Science 279*, 498−499.
4. Berens, R. L., Krug, E. C., and Marr, J. J. (1995) in *Biochemistry of Parasitic Organisms and Its Molecular Foundations* (Marr, J. J., and Muller, M., Eds.) pp 89−117, Academic Press, London.
5. Berman, P. A., Human, L., and Freese, J. A. (1991) *J. Clin. Invest. 88*, 1848−1855.
6. Somoza, J. R., Chin, M. S., Foda, P. J., Wang, C. C., and Fletterick, R. J. (1996) *Biochemistry 35*, 7032−7040.
7. Rossiter, B. J. F., and Caskey, C. T. (1995) in *The Metabolic and Molecular Bases of Inherited Disease* (Scriver, C. R., Beaudet, A. L., Sly, W. S., and Valle, D. Eds.) 7th ed., Vol. II, pp 1679−1706, McGraw-Hill, Inc., New York.
8. Li, C. M., Tyler, P. C., Furneaux, R. H., Kicska, G., Xu, Y., Grubmeyer, C., Girvin, M. E., and Schramm, V. L. (1999) *Nat. Struct. Biol. 6*, 582−587.
9. Tso, W., Grubmeyer, C., and Blanchard, J. S. (1996) *Biochemistry 35*, 14−21.
10. Kline, P. C., and Schramm, V. L. (1993) *Biochemistry 32*, 13212−13219.
11. Schramm, V. L. (1998) *Annu. Rev. Biochem. 67*, 693−720.
12. Shi, W., Li, C. M., Tyler, P. C., Furneaux, R. H., Grubmeyer, C., Schramm, V. L., and Almo, S. C. (1999) *Nat. Struct. Biol. 6*, 588−593.
13. Otwinowski, Z., and Minor, W. (1997) *Methods Enzymol. 276*, 307−326.
14. Navaza, J. (1994) *Acta Crystallogr. A50*, 157−163.
15. Brunger, A. T. (1992) *X-PLOR Version 3.1*, Yale University Press, New Haven, CT.
16. Jones, T. A. (1985) *Methods Enzymol. B115*, 157−171.
17. Laskowski, R. A., MacArthur, M. W., Moss, D. S., and Thornton, J. M. (1993) *J. Appl. Crystallogr. 26*, 283−291.
18. Focia, P. J., Craig, S. P., III, and Eakin, A. E. (1998) *Biochemistry 37*, 17102−17127.
19. Horenstein, B. A., and Schramm, V. L. (1993) *Biochemistry 32*, 7089−7097.
20. Xu, Y., Eads, J., Sacchettini, J. C., and Grubmeyer, C. (1997) *Biochemistry 36*, 3700−3712.
21. Eads, J. C., Scapin, G., Xu, Y., Grubmeyer, C., and Sacchettini, J. C. (1994) *Cell 78*, 325−334.
22. Xu, Y., and Grubmeyer, C. (1998) *Biochemistry 37*, 4114−4124.
23. McDermott, A., and Ridenour, C. F. (1996) in *Encyclopedia of NMR*, pp 3820−3825, J. Wiley & Sons Ltd., Sussex, England.
24. McDermott, A., and Wei, Y. (1999) in *Modeling NMR Chemical Shifts: Giving Insight Into Structure and Environment* (Facelli, J., and de Dias, A. Eds.) American Chemical Society, Washington, DC (in press).
25. Cleland, W. W., and Kreevoy, M. M. (1994) *Science 264*, 1887−1890.
26. Horenstein, B. A., and Schramm, V. L. (1993) *Biochemistry 32*, 9917−9925.
27. Parkin, D. W., and Schramm, V. L. (1995) *Biochemistry 34*, 13961−13966.
28. Evan, S. V. (1993) *J. Mol. Graphics 11*, 134−138.
29. Plateau, P., and Gueron, M. (1982) *J. Am. Chem. Soc. 104*, 7310−7311.

BI990664P